Engineering and Technology Journal e-ISSN: 2456-3358

Volume 10 Issue 11 November 2025, Page No.- 7742-7751

DOI: 10.47191/etj/v10i11.06, I.F. – 8.482

Assessing Prevalent Open-Source Insar Time Series Analysis Methods for Ground Subsidence Monitoring In Midvaal, South Africa

Thobani Maluleka[1], Siphiwe Mphuthi[2]

[1]Architecture Planning and Geomatics, University of Cape Town, Cape Town, South Africa

[2]Geospatial Research and Innovations, EarthSense Geospatial Inc., Johannesburg, South Africa

ABSTRACT: Ground subsidence is a growing geohazard in the Midvaal region of South Africa, threatening infrastructure, economic activities, and community well-being. Current monitoring techniques often lack the necessary spatial and temporal resolution, highlighting an urgent need for more precise and efficient methods. This study investigates the effectiveness of prevalent open-source Interferometric Synthetic Aperture Radar (InSAR) time series analysis methods and tools for monitoring ground subsidence in Midvaal. We used Sentinel-1 Single Look Complex imagery from January 2019 to December 2021 and evaluated four distinct InSAR workflows: Persistent Scatterer (PS) InSAR using ISCE–StaMPS and SNAP–StaMPS, Small Baseline Subset (SBAS) InSAR using ISCE–StaMPS and HyP3–MintPy. The AW3D, 30m resolution DEM was used for topographic phase correction, and continuous Global Navigation Satellite System (cGNSS) data from Heidelberg (HEID) and Vereeniging (VERG) stations validated InSAR-derived Line-of-Sight (LOS) velocities using metrics like Root Mean Square Error (RMSE), Mean Absolute Error (MAE), and Range Error. Our results show clear spatial patterns of ground deformation, with ground subsidence concentrated in the northeastern and southeastern regions and uplift in the northwestern region. ISCE-StaMPS PS-InSAR and SBAS-InSAR demonstrated the highest precision with the lowest standard errors, making them suitable for detecting subtle movements. In contrast, HyP3-MintPy SBAS-InSAR, while exhibiting larger standard errors, proved valuable for capturing broader, large-scale deformations, including extreme ground subsidence rates of up to -233.9 mm/year. Correlation analysis revealed a strong positive correlation of 0.7 between ISCE-StaMPS and SNAP-StaMPS PS-InSAR, while other method pairs showed weaker correlations, indicating differences in the type of scatterers, distinct strengths and limitations. Velocity accuracy evaluation against cGNSS data showed that ISCE-StaMPS SBAS-InSAR and SNAP-StaMPS PS-InSAR achieved the lowest MAE and RMSE, meeting the NISAR mission's validation criterion for secular ground deformation. This research underscores the importance of method selection based on specific study objectives, whether high precision or broad spatial coverage is prioritized, and highlights the need for continued refinement of InSAR techniques for accurate geohazard monitoring in dynamic environments.

KEYWORDS: Ground Subsidence, Insar Time Series Analysis, SBAS-Insar, PS-Insar

I. INTRODUCTION

Ground subsidence represents a critical geohazard that affects urban and peri-urban areas worldwide, with consequences ranging from infrastructure damage to significant safety risks for human settlements [1]. In South Africa, the Midvaal region of Gauteng has experienced a growing incidence of ground subsidence, posing a direct threat to vital infrastructure, economic activities, and community well-being [2], [3], [4]. Despite the severity of this issue, current monitoring and mitigation strategies often rely on conventional techniques, which are frequently constrained by limited spatial and temporal resolution, as well as delayed reporting of ground subsidence patterns [5]. These shortcomings highlight the urgent need for innovative, data driven approaches that can enhance the precision and efficiency of ground subsidence monitoring.

Interferometric Synthetic Aperture Radar (InSAR) time series analysis has emerged as a transformative technology for monitoring ground deformation [6], [7], [8]. Its capability to detect millimetre surface movements across extensive areas, combined with high temporal and spatial resolution, makes it particularly well-suited for addressing ground subsidence challenges [5], [9].

Nevertheless, a significant barrier to its widespread application lies in the variability of tools and methodologies available for InSAR data processing. Different software packages, algorithmic frameworks, and parameter configurations can yield divergent results, complicating efforts to standardize and validate findings. This variability necessitates a systematic evaluation of InSAR time series techniques to determine their reliability and applicability, particularly in regions like Midvaal where precise ground subsidence monitoring is indispensable.

This study seeks to bridge these gaps by investigating the effectiveness of various open-source InSAR time series analysis tools and methods for monitoring ground subsidence in Midvaal. By examining the performance, accuracy, and practicality of these tools, the research aims to provide insights into their suitability for addressing ground subsidence related challenges in the South African context. The study not only contributes to advancing geospatial methodologies but also underscores the role of modern technologies in tackling geohazards. By focusing on the technical and practical aspects of InSAR time series analysis, it aims to inform future research and operational practices, paving the way for improved monitoring, mitigation, and decision-making in regions susceptible to ground subsidence.

II. MATERIALS AND METHODS

A. Study Area

This study is conducted in Midvaal, located in the northeastern region of South Africa, with coordinates ranging from 26° 18' 38'' S to 26° 56' 53'' S in latitude and 27° 50' 40'' E to 28° 25' 52'' E in longitude. Spanning approximately 4,126.34 square kilometres, Midvaal is a highly populated rural-urban area, home to 112,254 residents as of 2022.

The region's geological landscape is notably diverse, with dolomite formations being particularly vulnerable to pollution and ground subsidence, which pose significant challenges to sustainability [2], [10]. Additionally, rapid urbanization, agricultural and industrial expansion have exerted considerable strain on Midvaal's water resources, leading to concerns about excessive groundwater extraction, ground subsidence, and the emergence of sinkholes. Figure 1. provides a comprehensive map of the region's geographical boundaries, elevation and geological features, illustrating the geological and topographic complexities of the area.

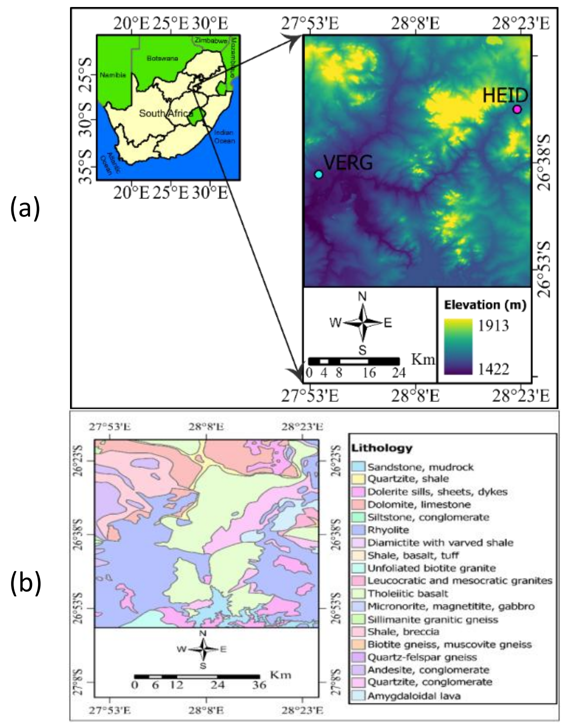

Figure 1. Geographical location and, (a) elevation and (b) geological features of Midvaal, South Africa.

B. Datasets

This study used a combination of satellite-based and ground-based datasets to monitor ground deformation within the study area. The primary dataset was Sentinel-1 Single Look Complex (SLC) imagery acquired in descending interferometric wide (IW) mode, from the Alaska Satellite Facility (ASF) Distributed Active Archive Center (DAAC). Sentinel-1's C-band was selected due to its high temporal resolution (12-day revisit cycle post-2017), wide swath coverage (250 km in IW mode), and proven ability to detect ground deformation even in vegetated or agricultural regions. A total of 84 descending orbit images spanning January 2019 to December 2021 were used, centred consistently on frame 677 (path 50), ensuring coherence and comparability across the time series.

To correct for topographic phase and support interferometric processing, the "Advanced Land Observing Satellite World 3D" 30 meters resolution (AW3D30) Digital Elevation Model (DEM) was used. This 30 m resolution DEM, referenced to World Geodetic System 1984 (WGS84) and Earth Gravitational Model 1996 (EGM96), was selected based on existing literature [11] highlighting its demonstrated superior performance in South African conditions, and offering enhanced vertical accuracy over other publicly available DEM's.

The validation of InSAR-derived Line-of-Sight (LOS) velocities was performed using continuous Global Navigation Satellite System (cGNSS) station data from Heidelberg (HEID) and Vereeniging (VERG). These cGNSS/TrigNet stations, operated by the Chief Directorate: National Geospatial Information (CD: NGI) and processed by the Nevada Geodetic Laboratory (NGL), provided East-North-Up (ENU) displacement time series data. Comparison with satellite InSAR derived velocities enabled independent verification of ground deformation trends and detection of any discrepancies due to processing errors or localized environmental factors. It is noted that these two stations represent the only ground-based geodetic infrastructure available for independent validation in this region, thus some limitation due to spatial underrepresentation. Despite this constraint, the cGNSS data still provides crucial point-based validation of the Line-of-Sight velocities, contributing to the overall assessment of method accuracy.

C. InSAR Processing Techniques

To assess the impact of various InSAR pre-processing, processing, and time series analysis techniques on the detection of ground deformation across the study area, four distinct workflows were implemented. The first workflow employed the Persistent Scatterer (PS) technique using the InSAR Scientific Computing Environment (ISCE) in combination with the Stanford Method for Persistent Scatterers (StaMPS). The second used the Small Baseline Subset (SBAS) approach, also integrating ISCE and StaMPS. The third applied the PS method using the SeNtinel

Application Platform (SNAP) together with StaMPS. Lastly, the fourth workflow incorporated the ASF Hybrid Pluggable Processing Pipeline (HyP3) with the Miami InSAR Time-series software in Python (MintPy) [12], [13], [14], [15], [16], [17]. These methods were chosen to capture both localized and regional patterns of ground deformation while enabling cross-validation of results through methodological redundancy.

1. PS-InSAR (ISCE–StaMPS)

This approach involved generating wrapped interferograms using the InSAR Scientific Computing Environment, which were then converted into StaMPS-compatible format. In StaMPS, coherent permanent scatterers were identified based on amplitude dispersion and phase stability. Phase unwrapping was carried out using SNAPHU, and spatially uncorrelated look angle errors were corrected. Additional corrections addressed errors arising from DEM inaccuracies, atmospheric effects, and satellite orbit mismatches. And the atmospheric phase delays were filtered using the TRAIN toolbox to improve the accuracy of the final velocity estimates by mitigating atmospheric phase delays.

2. SBAS-InSAR (ISCE–StaMPS)

This workflow used ISCE to generate a network of small baseline interferograms, which were then processed in StaMPS to derive ground displacement over time. The method optimized interferogram selection for temporal and spatial coherence. Corrections were applied for unwrapping errors and atmospheric delays, and average velocities were estimated using least-squares inversion of the time-series data. This method proved effective for mapping broad-scale ground deformation patterns.

3. PS-InSAR (SNAP–StaMPS)

In this workflow, interferograms were generated using the Sentinel Application Platform, developed by European Space Agency (ESA). The results were then formatted for StaMPS, where PS-InSAR analysis was performed. The processing steps were similar to those in the ISCE–StaMPS PS-InSAR workflow, including scatterer selection, phase unwrapping, and atmospheric correction. This alternative processing path served to validate the consistency and reliability of PS-InSAR results obtained from different pre-processing tools and methods.

4. SBAS-InSAR (HyP3–MintPy)

This method involved the use of ASF HyP3 platform to generate unwrapped interferograms, which were then analysed using MintPy. Key processing steps included network refinement, tropospheric delay correction, and removal of topographic and unwrapping errors. Reference point selection and optimization of the interferometric network were also performed prior to velocity estimation. The approach was efficient for detecting gradual, spatially extensive ground deformation signals.

Together, these methods enabled the generation of InSAR time-series analysis ground deformation maps and average velocity fields. Cross comparison between the outputs provided insights into the strengths and limitations of each approach, methods and reinforced the reliability of the detected ground deformation trends.

D. Correlation Analysis

To evaluate the level of agreement between the different InSAR time series analysis processing techniques, Pearson correlation analysis was applied to the velocity maps generated by ISCE-StaMPS PS-InSAR, ISCE-StaMPS SBAS-InSAR, SNAP-StaMPS PS-InSAR, and HyP3-MintPy SBAS-InSAR. All velocity outputs were converted into 3 arc-second raster grids using the stamps_to_raster and h5_to_raster modules within the StoSAP processor. StaMPS CSV files were first mapped to grid pixels based on geographic coordinates, while MintPy H5 outputs were aligned using a reference raster with EPSG:4326 projection. Once coregistered, the rasters were compared on a pixel-by-pixel basis using only the common spatial extent across all methods. Pearson correlation coefficients were calculated to quantify the relationships and used to visualize the consistency between datasets.

E. Frequency Distribution Analysis

A frequency distribution analysis was performed using the common grid pixels across all four InSAR time series analysis methods to characterize the distribution of ground deformation velocity values. The gridded data were classified into predefined velocity intervals, and the number of occurrences within each class was tallied. This procedure was used to observe how each InSAR time series analysis method represented spatial patterns in the ground deformation velocity field and to assess variation in the distribution of measured ground displacements.

F. Accuracy Evaluation

The accuracy of InSAR time series analysis derived ground deformation velocities was assessed by comparing them with data from two continuous GNSS stations, the Heidelberg and Vereeniging stations. For StaMPS-based inherent point-based outputs, cGNSS comparison was conducted by interpolating the average velocity from the 25 nearest PS/SBAS points located within a 2 km radius of each station using the stamps_nearby module within the StoSAP processor. For MintPy-based gridded results, raster values at the station coordinates were extracted using the 'Extract Multi Values to Points' tool in ArcPy after converting the H5 files into raster format. While the velocity extraction/interpolation methods differ, they are chosen to be most suitable for the respective data structures produced by each InSAR software. Subsequently, accuracy was conducted using metrics such as Root Mean Square Error (RMSE), Mean Absolute Error (MAE), and Range Error. These metrics were computed to quantify the difference between cGNSS and InSAR time series analysis estimates.

G. Baseline Error Comparison

The baseline velocity error evaluation was undertaken to determine the effectiveness of each InSAR time series analysis method in capturing long-term, stable ground deformation. This assessment involved comparing the linear (secular) velocities derived from InSAR with those obtained from continuous GNSS (cGNSS) stations, with the aim of evaluating consistency within a defined accuracy threshold. The validation followed standards similar to those prescribed by satellite missions such as 'National Aeronautics and Space Administration' (NASA) – 'Indian Space Research Organization' (ISRO) Synthetic Aperture Radar (NISAR), which require InSAR-derived measurements to achieve an accuracy of 2 mm/year for secular deformation or $3 \times (1 + L^{1/2})$ mm/year for transient deformation, where L is the baseline length in kilometres within the range of 0.1 km to 50 km. These thresholds provide a benchmark for determining whether the observed differences between InSAR and cGNSS velocity estimates fall within acceptable limits for mission-level validation and long-term geophysical interpretations.

III. RESULTS

A. Ground Deformation Pattern

The velocity maps derived from the different methods and software showed clear spatial patterns of ground deformation across the study area (Figure 2.). Ground subsidence was predominantly observed in the northeastern and southeastern regions, while uplift was more localized in the northwestern region. Specifically, the maximum ground subsidence rate observed in the ISCE-StaMPS PS-InSAR processing was -8.7 mm/year, while the maximum ground uplift rate reached 2.7 mm/year. The standard errors of these measurements ranged from 0.1 mm/year to 1.0 mm/year, reflecting the accuracy of the PS-InSAR method. In contrast, the ISCE-StaMPS SBAS-InSAR method revealed more extensive areas of ground subsidence, with a maximum rate of -25.8 mm/year in the northern, southwestern, and eastern regions, and significant ground uplift of up to 27.8 mm/year in the southeastern area. Standard errors for this method ranged from 0.1 mm/year to 3.5 mm/year, showing a wider variability in the results.

SNAP-StaMPS PS-InSAR also showed ground subsidence in the southeastern part of the study area, with maximum ground subsidence of -6.4 mm/year and ground uplift of 1.8 mm/year. The standard errors ranged from 0.1 mm/year to 1.3 mm/year, similar to ISCE-StaMPS PS-InSAR but with slightly higher errors. For HyP3-MintPy SBAS-InSAR, ground subsidence was observed in the southeastern, northeastern, and southwestern parts of the study area, with the maximum ground subsidence rate reaching -233.9 mm/year and maximum ground uplift of 49.2 mm/year. Standard errors for this method ranged from 0.0 mm/year to 5.4 mm/year, reflecting both the large-scale ground deformation observed and the higher variability in measurements. The extreme ground subsidence rates are often associated with highly localized phenomena that may include active mining, intense groundwater extraction, or localized geological instabilities, which are prevalent in parts of the Midvaal region.

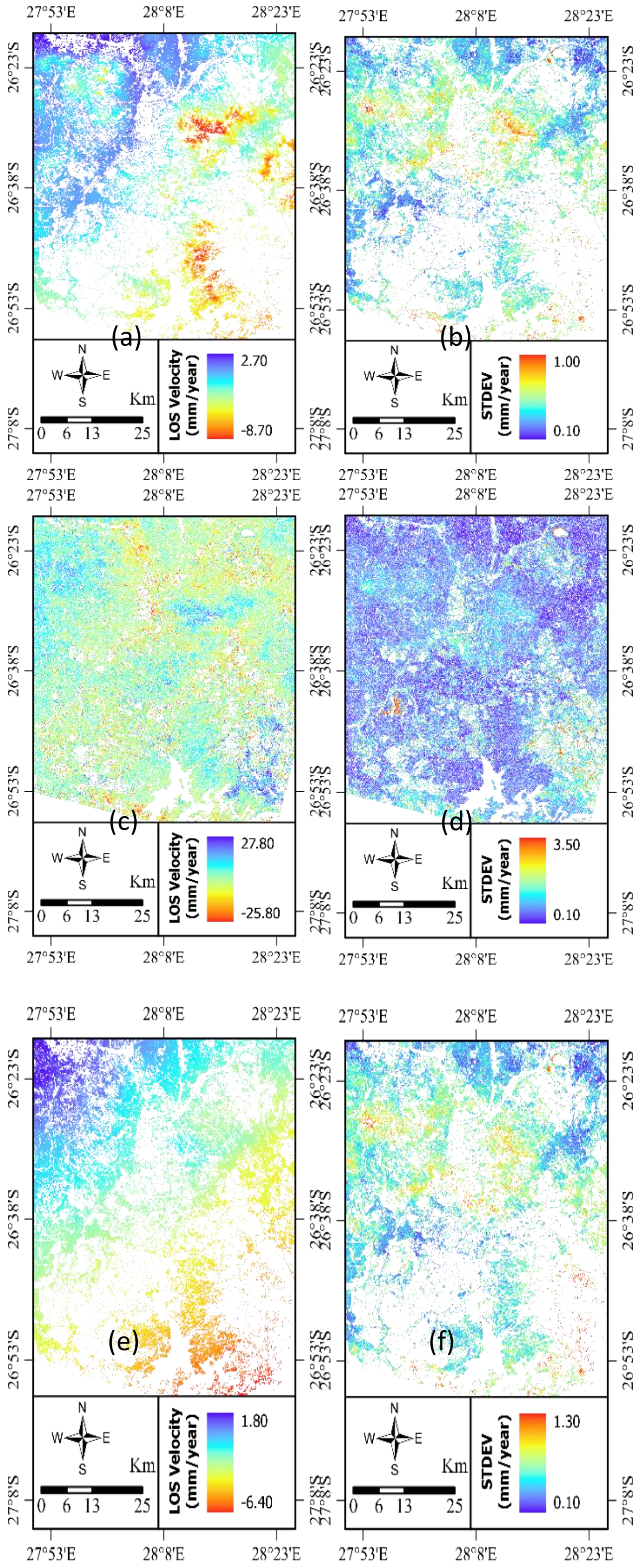

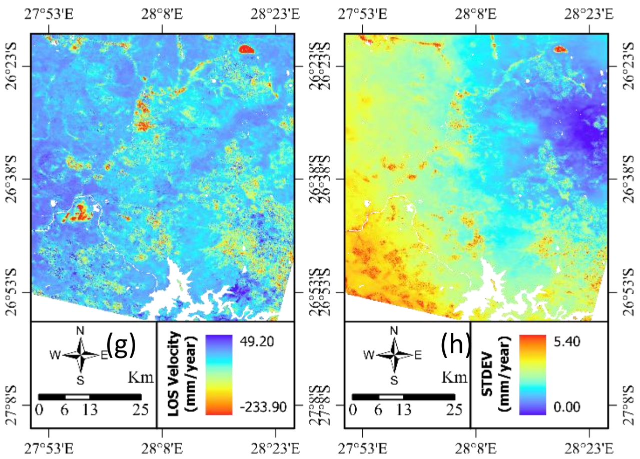

Figure 2. Ground deformation velocity and their corresponding velocity standard error maps obtained from, (a, b) ISCE-StaMPS PS-InSAR, (c, d) ISCE-StaMPS SBAS-InSAR, (e, f) SNAP-StaMPS PS-InSAR, (g, h) HyP3-MintPy SBAS-InSAR.

B. Correlation Between Methods

The Pearson correlation analysis between the different InSAR time series analysis methods revealed notable trends (Figure 3. And Figure 4.). ISCE-StaMPS and SNAP-StaMPS PS-InSAR showed the strongest positive correlation of 0.70 with a best-fit slope of 0.48, indicating similar behaviour in ground deformation measurement and type of scatterers. By contrast, the correlation between ISCE-StaMPS PS-InSAR and HyP3-MintPy SBAS-InSAR was weak at 0.27 with a slope of 0.40, highlighting methodological differences and variations in their ability to capture deformation patterns. ISCE-StaMPS PS-InSAR and ISCE SBAS-InSAR showed a weak negative correlation (-0.13) with a negative slope (-0.15), underscoring contrasting PS and DS point characteristics. Similarly, SNAP-StaMPS PS-InSAR and HyP3-MintPy SBAS-InSAR showed a weak positive correlation of 0.19 (slope 0.41), while SNAP-StaMPS PS-InSAR and ISCE SBAS-InSAR had a weak positive correlation of 0.23 (slope 0.38). The weakest correlation was observed between HyP3-MintPy SBAS-InSAR and ISCE SBAS-InSAR (0.11, slope 0.08), where points were symmetrically distributed about the best-fit line but formed an oval-shaped cluster, suggesting strong non-linear patterns and tool-related differences.

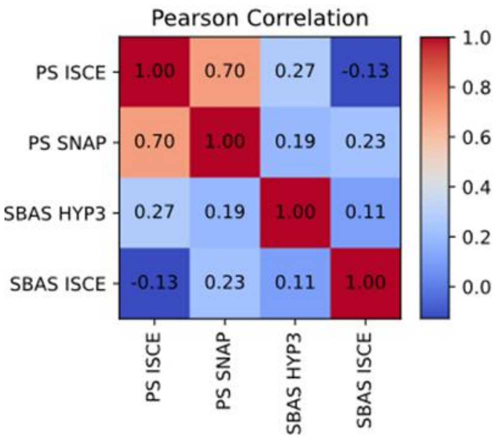

Figure 3. Techniques and Tools Pearson correlation.

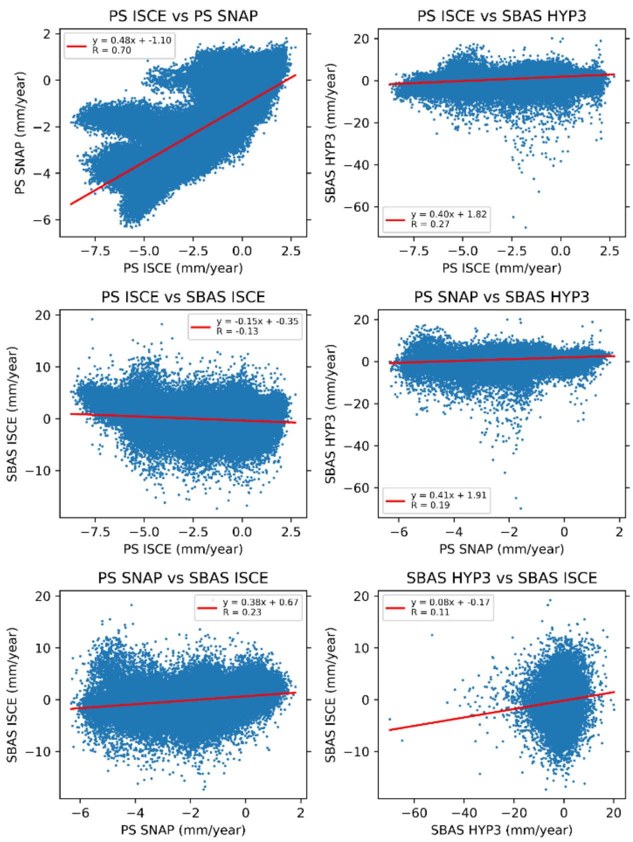

Figure 4. Correlation scatter plots between InSAR techniques and tools, showing best-fit lines, clustering behaviour, and differences in velocity range capture.

Overall, the scatter plots (Figure 4.) demonstrate that while all techniques produce point clusters along best-fit lines, their clustering patterns vary. HyP3-MintPy SBAS-InSAR and ISCE-StaMPS SBAS-InSAR are particularly concentrated within -20 mm/yr to 20 mm/yr, which underscores their limited ability to capture higher-magnitude velocities compared to HyP3-MintPy SBAS-InSAR, which detects deformation beyond ±30 mm/yr. These variations align with the velocity maps and highlight how methodological and tool-based differences influence the detection and interpretation of ground subsidence signals.

C. Frequency Distribution of Velocities

Leveraging the common pixel points among all techniques, we plotted the frequency distribution of the velocities to understand their class patterns (Figure 5.). ISCE-StaMPS PS-InSAR, HyP3-MintPy SBAS-InSAR, and ISCE-StaMPS SBAS-InSAR showed higher velocity frequencies at 0 mm/year, except for SNAP-StaMPS PS-InSAR, which displayed the highest frequency at around -2 mm/year. This indicates that velocities between ISCE-StaMPS PS-InSAR, HyP3-MintPy SBAS-InSAR, and ISCE-StaMPS SBAS-InSAR are similar and different from SNAP-StaMPS PS-InSAR, which may indicate errors in the SNAP-StaMPS PS-InSAR technique. All four techniques showed positively skewed velocities, though ISCE-StaMPS and HyP3-MintPy SBAS-InSAR showed much better normal distribution patterns.

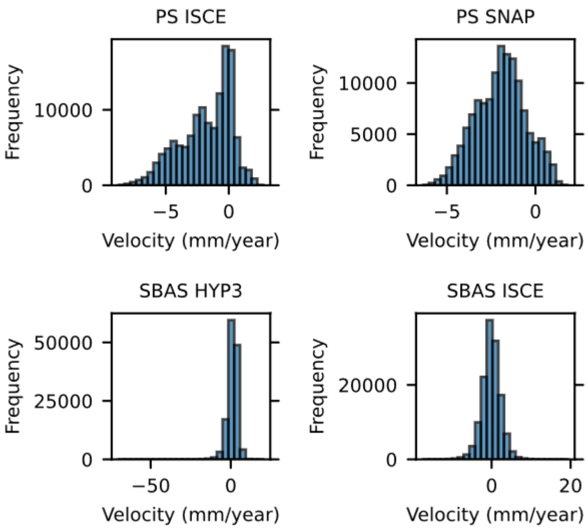

Figure 5. Techniques and tools frequency distribution.

D. Velocity Accuracy Evaluation

Velocity accuracy evaluation was conducted by comparing the InSAR time series analysis derived velocities with data from continuous GNSS stations (HEID and VERG) (Figure 6.). The results revealed notable differences in performance across the processing methods and software used. SNAP-StaMPS PS-InSAR exhibited the highest relative velocity errors at both validation stations, 10.0 mm/year at HEID and 8.0 mm/year at VERG. In contrast, ISCE-StaMPS SBAS-InSAR demonstrated better alignment with cGNSS-derived velocities, likely due to its effectiveness in mitigating phase unwrapping and atmospheric delay errors, which commonly affect PS processing in heterogeneous or low-coherence environments. Overall, HyP3-MintPy SBAS-InSAR showed the best performance among the tested methods.

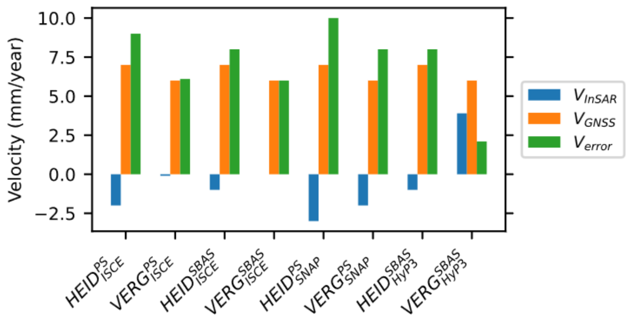

Figure 6. Relative LOS Velocity differences between cGNSS and InSAR implied.

HyP3-MintPy SBAS-InSAR, while capable of capturing a broader range of ground deformation velocities, including extreme displacements, showed the largest standard error values, particularly in the western part of the study area, where errors reached up to ±5.4 mm/year. At station VERG, HyP3-MintPy SBAS-InSAR reported a large absolute velocity error of −5.9 mm/year, consistent with the standard error map and suggesting potential limitations for precise velocity estimation at that location. ISCE-StaMPS PS-InSAR also performed poorly at VERG, further indicating that site-specific factors such as atmospheric heterogeneity or local surface characteristics may negatively impact Persistent Scatterer analysis in that area.

Based on the absolute comparison after georeferencing and adjusting the InSAR-derived velocities using station HEID, the performance of the methods was reassessed with reference to station VERG (Figure 7.). Under this framework, ISCE-StaMPS SBAS-InSAR and SNAP-StaMPS PS-InSAR exhibited the best agreement with the cGNSS observations, followed by ISCE-StaMPS PS-InSAR, while HyP3-MintPy SBAS-InSAR performed the weakest. The importance of georeferenced results lies in their ability to provide absolute velocity estimates that are consistent across the study area, thereby improving the reliability of inter-station comparisons and enabling integration with other geodetic datasets. The variation in performance across methods can also be attributed to the type and distribution of scatterers; Persistent Scatterer techniques such as SNAP-StaMPS PS-InSAR, generally rely on bright, stable point targets (e.g., buildings or rock outcrops), whereas Small Baseline approaches, like ISCE-StaMPS and HyP3-MintPy SBAS-InSAR incorporate distributed scatterers, which may be more sensitive to decorrelation in heterogeneous or vegetated environments. These differences in scatterer characteristics directly influence error propagation and explain the contrasting behaviour observed at station VERG.

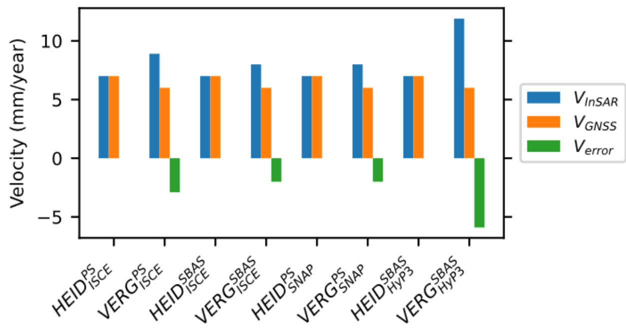

Figure 7. Absolute LOS Velocity differences between cGNSS and InSAR implied.

Additionally, statistical analysis of the absolute velocity differences confirmed these trends (Table 1.). ISCE-StaMPS SBAS-InSAR and SNAP-StaMPS PS-InSAR both yielded the lowest mean absolute error (1.0 mm/year), narrowest error range (2.0 mm/year), and lowest RMSE (1.4 mm/year), indicating their suitability for applications requiring precise detection of subtle, long-term ground movements, such as tectonic plate monitoring. Conversely, HyP3-MintPy SBAS-InSAR recorded the highest RMSE (4.2 mm/year), widest error range (5.9 mm/year), and largest mean absolute error

(3.0 mm/year), reflecting lower precision despite its broader deformation detection capability.

Table 1. Absolute Velocity differences statistics (units: mm/year).

Metric	Persistent Scatter		Small Baseline Subset	
	$ISCE_{StaMPS}$	$SNAP_{StaMPS}$	$ISCE_{StaMPS}$	$HyP3_{MintPy}$
MAE	1.5	1.0	1.0	3.0
Range	2.9	2.0	2.0	5.9
RMSE	2.1	1.4	1.4	4.2

E. Baseline Error Comparison

The baseline error comparisons between the InSAR time series analysis derived velocities and cGNSS data revealed that ISCE-StaMPS SBAS-InSAR and SNAP-StaMPS PS-InSAR met the NISAR mission's validation criterion of ±2 mm/year for long-term (secular) ground deformation (Table 2.). In contrast, ISCE-StaMPS PS-InSAR and HyP3-MintPy SBAS-InSAR exceeded this threshold, indicating reduced accuracy in detecting stable motion. Despite these differences in secular accuracy, all four InSAR methods complied with the NISAR-defined threshold for transient deformation of ±24.16 mm/year over spatial baselines from 0.1 km to 50 km. This suggests that each method remains capable of identifying short-term or highly localized ground displacement events across the study area.

Table 2. Baseline (HEID-VERG) LOS velocity differences between cGNSS and InSAR implied (units: mm/year).

Method ID	Baseline Error	Distance (km)	NISAR Error Threshold
$ISCE_{PS}$	2.9	49.73	24.16
$ISCE_{SBAS}$	2.0	49.73	24.16
$SNAP_{PS}$	2.0	49.73	24.16
$HyP3_{SBAS}$	5.9	49.73	24.16

Caveat: The provided MAE, RMSE, and Range values are point estimates derived from the limited cGNSS stations available for this large study area.

IV. DISCUSSION

A. Comparison of Ground Deformation Patterns

The analysis of ground deformation patterns derived from the different InSAR time series analysis methods indicate clear spatial variations in the measurements. Each method captured ground subsidence and ground uplift differently across the study area. The ISCE-StaMPS PS-InSAR technique, which showed precise measurements with lower standard errors, captured ground subsidence and ground uplift predominantly in the northeastern and southeastern regions. This suggests that the technique's precision makes it suitable for monitoring areas where ground deformation is subtle and requires accurate detection.

In contrast, the ISCE-StaMPS SBAS-InSAR method highlighted broader areas of ground subsidence, including significant regions in the northern, southwestern, and eastern parts of the study area, as well as localized ground uplift. The higher standard errors associated with this technique suggest that while it is more robust for large-scale ground subsidence mapping, it may be less precise than ISCE-StaMPS PS-InSAR, particularly in areas with low ground deformation rates.

SNAP-StaMPS PS-InSAR also identified ground subsidence in the southeastern part of the study area, with slightly higher errors compared to ISCE-StaMPS PS-InSAR. This could be attributed to differences in phase unwrapping algorithms and atmospheric correction methods, which might explain the slight discrepancies observed in the velocities. Finally, HyP3-MintPy SBAS-InSAR, with its broad spatial coverage, detected extreme values of ground deformation, including a maximum ground subsidence rate of -233.9 mm/year. While this high variability in deformation velocities reflects the method's sensitivity to large-scale movement, it also suggests the method's potential limitations in detecting smaller, localized deformations with precision. Furthermore, localized investigations employing ground-truth surveys or high-resolution optical imagery are required to definitively confirm the specific causes of these extreme deformation rates.

B. Evaluation of Technique Precision

The precision of each InSAR time series analysis technique is crucial for accurate ground deformation analysis. The results showed that ISCE-StaMPS PS-InSAR and SBAS-InSAR exhibited the lowest standard errors, making them the most precise methods for measuring ground subsidence and uplift, capturing both persistent and distributed scatterers. This is consistent with previous studies which have highlighted ISCE-StaMPS robust algorithms for handling various ground deformation mechanisms [5]. SNAP-StaMPS PS-InSAR, while slightly less precise, still provided valuable data but with higher standard errors, potentially due to less sophisticated phase unwrapping methods compared to ISCE-StaMPS PS-InSAR.

HyP3-MintPy SBAS-InSAR demonstrated larger standard errors, yet its ability to capture a wide range of deformation velocities makes it a powerful tool for detecting more significant changes in ground displacements. However, the method's lower precision suggests that it may be better suited for identifying large ground deformation patterns rather than subtle or localized ground movements. The unique strengths of each technique underline the importance of selecting the appropriate method based on the specific requirements of a given study, whether precision or the ability to detect large-scale ground deformation is prioritized.

C. Frequency Distribution and Statistical Analysis

The frequency distribution of velocities across all techniques provided important insights into the performance of each method. The observation that ISCE-StaMPS PS-InSAR, HyP3-MintPy SBAS-InSAR, and ISCE-StaMPS SBAS-InSAR displayed higher frequency distributions at 0 mm/year, while SNAP-StaMPS PS-InSAR peaked around -2 mm/year, suggesting that SNAP-StaMPS PS-InSAR might be more prone to errors, particularly in cases of low ground deformation. This -2 mm/year peak could also have introduced bias in the accuracy assessment, potentially making SNAP-StaMPS PS-InSAR appear more accurate than it actually is when compared to a limited set of validation stations. Incorporating additional validation stations in future analyses would help to reveal and mitigate such biases more effectively, providing a more robust evaluation of method performance. Additionally, the similarity between ISCE-StaMPS PS-InSAR, ISCE-StaMPS SBAS-InSAR, and HyP3-MintPy SBAS-InSAR velocities indicate that these methods can capture similar patterns of ground motion, although their precision differs.

The positively skewed distribution of velocities for all methods further supports the notion that ground subsidence is more prevalent in the study area than ground uplift, with the distribution of velocities tending to cluster towards lower ground de-formation rates. ISCE-StaMPS and HyP3-MintPy SBAS-InSAR, which showed better normal distribution patterns, suggest that these methods could be more reliable for analysing ground deformation at the regional level, where trends can be expected to follow more predictable patterns.

D. Accuracy and Error Assessment

The accuracy evaluation revealed that ISCE-StaMPS SBAS-InSAR and SNAP-StaMPS PS-InSAR were more accurate when compared to cGNSS data, with errors remaining within the expected range for secular ground deformation. HyP3-MintPy SBAS-InSAR, while showing the least performance in relative accuracy, nonetheless maintained error values within its reported standard error ranges. This indicates that HyP3-MintPy is a robust approach as its accuracy and associated uncertainties reflect realistic estimates and errors, thereby providing a reliable representation of ground deformation magnitudes. Moreover, despite its larger standard errors, HyP3-MintPy SBAS-InSAR was able to capture large-scale ground deformation, particularly in regions with significant ground subsidence. This finding underscores the importance of conducting accuracy assessments to evaluate the reliability of InSAR-based measurements, especially when monitoring large or highly dynamic regions subject to tectonic or anthropogenic influences

The differences in accuracy between methods further emphasize the need for a comprehensive validation strategy that includes both remote sensing data and ground-based observations, such as GNSS measurements to fully assess the performance of each technique. Additionally, the ability to detect small-scale ground movements in areas with relatively low ground deformation rates remains a challenge for many InSAR techniques, as evidenced by the larger error margins in methods like HyP3-MintPy SBAS-InSAR. Furthermore, the HyP3-MintPy's SBAS-InSAR broader detection capability, while valuable for large-scale changes might inherently be more susceptible to phase unwrapping ambiguities or regions of high temporal decorrelation compared to PS-InSAR methods, especially in areas of rapid and severe deformation.

V. CONCLUSION

This study has demonstrated the utility and challenges of various InSAR processing techniques in monitoring ground subsidence and uplift. By comparing ISCE-StaMPS PS-InSAR, SNAP-StaMPS PS-InSAR, ISCE-StaMPS SBAS-InSAR, and HyP3-MintPy SBAS-InSAR, the results reveal that each method offers unique advantages depending on the scale and precision required. ISCE-StaMPS PS-InSAR and SBAS-InSAR emerged as the most precise, while HyP3-MintPy SBAS-InSAR proved valuable in detecting large-scale ground deformations. The differences in accuracy and standard errors across these methods highlight the importance of choosing the appropriate technique based on specific study objectives, whether precision or broader spatial coverage is prioritized. The findings of this study underscore the need for careful selection of InSAR methods and tools, as each method provides distinct insights into ground deformation. The ability to monitor both large and subtle ground deformations is critical for applications ranging from urban planning to earthquake monitoring. However, the limitations of these methods, particularly in handling small-scale ground deformations with high accuracy, suggest that further improvements are necessary.

Future research should focus on enhancing the accuracy and reliability of techniques like HyP3-MintPy SBAS-InSAR. While HyP3-MintPy demonstrated robustness by maintaining accuracy within its reported standard error ranges, further refinement is needed to reduce relative performance gaps with StaMPS-based methods. Addressing limitations such as the potential bias introduced by the -2 mm/year peak in SNAP-StaMPS PS-InSAR, the sensitivity of PS approaches to site-specific scatterer types, and the influence of atmospheric heterogeneity on velocity estimates will be essential. Equally important is the assessment of DEM effects as residual topographic errors can propagate into interferometric phase signals, thereby influencing velocity accuracy in both PS and SBAS processing chains. In addition, expanding the number and spatial distribution of validation stations will help to detect and mitigate localized biases more effectively, ensuring stronger validation of InSAR-derived velocities. By refining these techniques and incorporating diverse datasets, InSAR can become more reliable and broadly applicable in dynamic and densely populated regions. Ultimately, a more comprehensive and accurate approach to ground deformation monitoring will provide better support for decision-making in areas affected by ground subsidence and uplift.

ACKNOWLEDGMENT

This research was supported by the Research Development Grant and the Postgraduate Funding Office at the UCT. The InSAR data used in this study were provided by ASF DAAC. The GNSS data was obtained from the Nevada Geodetic Laboratory, courtesy of CD:NGI, and the AW3D30 DEM was acquired from OpenTopography, courtesy of JAXA.

Computations were performed using facilities provided by the University of Cape Town's ICTS High Performance Computing team: hpc.uct.ac.za. The authors thank the UCT high Performance, the anonymous reviewers and the editor for their constructive comments.

DISCLOSURE STATEMENT

The author(s) declare no conflict of interest.

FUNDING

This work is supported by the University of Cape Town Research Development Grant and Postgraduate Funding Office. We are grateful for their support, and all views expressed here are those of the author(s) not the funding bodies.

NOTES ON CONTRIBUTORS

Thobani Maluleka:

Thobani Maluleka is a PhD candidate at the Division of Geomatics, University of Cape Town, South Africa. His research interests are geospatial data science and artificial intelligence, InSAR time series analysis, realization of geodetic reference frames, geoid modelling and gravity field analysis, data fusion, GIScience, remote sensing, environmental modelling, and capacity building in geospatial science and surveying.

Siphiwe M. Mphuthi:

Siphiwe Mphuthi is a Lecturer at the Division of Geomatics, University of Cape Town, South Africa. His research interests are physical geodesy, with a particular focus on gravimetric geoid modelling and the establishment of vertical datums. This encompasses the modernization of both horizontal and vertical geodetic reference frames, as well as the meticulous adjustment and analysis of gravity data.

ORCID

Thobani Maluleka – https://orcid.org/0000-0002-5156-2367

AUTHOR CONTRIBUTIONS

Thobani Maluleka – conceptualization, manuscript writing original draft, review and editing, methodology, data curation, investigation, visualization, formal analysis.

Siphiwe M. Mphuthi – conceptualization, manuscript review and editing, resources, validation, supervision.

DATA AVAILABILITY STATEMENT

The data that support the findings of this study are available from the corresponding author upon reasonable request.

REFERENCES

1. M. Bagheri-Gavkosh et al., 'Land subsidence: A global challenge', Science of The Total Environment, vol. 778, p. 146193, Jul. 2021, https://doi.org/10.1016/j.scitotenv.2021.146193.
2. A. Theron, J. Engelbrecht, J. Kemp, W. Kleynhans, and T. Turnbull, 'Detection of Sinkhole Precursors Through SAR Interferometry: Radar and Geological Considerations', IEEE Geosci. Remote Sensing Lett., vol. 14, no. 6, pp. 871–875, Jun. 2017, https://doi.org/10.1109/LGRS.2017.2684905.
3. H. Ashraf and F. Cawood, 'Geospatial subsidence hazard modelling at Sterkfontein Caves', SA J of Geomatics, vol. 4, no. 3, p. 273, Aug. 2015, https://doi.org/10.4314/sajg.v4i3.8.
4. T. Maluleka and S. M. Mphuthi, 'Assessing ground deformation monitoring techniques in Midvaal, South Africa', Journal of Applied Geodesy, Jun. 2025, https://doi.org/10.1515/jag-2024-0031.
5. P. Kirui, S. Oiro, H. Waithaka, P. Odera, B. Riedel, and M. Gerke, 'Detection, characterization, and analysis of land subsidence in Nairobi using InSAR', Nat Hazards, vol. 113, no. 1, pp. 213–236, Aug. 2022, https://doi.org/10.1007/s11069-022-05296-w.
6. L. Chai, X. Xie, C. Wang, G. Tang, and Z. Song, 'Ground subsidence risk assessment method using PS-InSAR and LightGBM: a case study of Shanghai metro network', International Journal of Digital Earth, vol. 17, no. 1, p. 2297842, Dec. 2024, https://doi.org/10.1080/17538947.2023.2297842.
7. X. Qiao et al., 'Interpretation and Attribution of Coastal Land Subsidence: An InSAR and Machine Learning Perspective', IEEE J. Sel. Top. Appl. Earth Observations Remote Sensing, vol. 17, pp. 4768–4783, 2024, https://doi.org/10.1109/JSTARS.2024.3361391.
8. H. Guo et al., 'Large-Scale Land Subsidence Monitoring and Prediction Based on SBAS-InSAR Technology with Time-Series Sentinel-1A Satellite Data', Remote Sensing, vol. 15, no. 11, p. 2843, May 2023, https://doi.org/10.3390/rs15112843.
9. W. L. Hakim, M. F. Fadhillah, S. Park, B. Pradhan, J.-S. Won, and C.-W. Lee, 'InSAR time-series analysis and susceptibility mapping for land subsidence in Semarang, Indonesia using convolutional neural network and support vector regression', Remote Sensing of Environment, vol. 287, p. 113453, Mar. 2023, https://doi.org/10.1016/j.rse.2023.113453.
10. S. Richardson, 'Sinkhole and subsidence record in the chuniespoort group dolomite, Gauteng, South Africa, Master's thesis. Pretoria: University of Pretoria, Department of Geology'. 2013.
11. M. Malindi and P. Odera, 'A new digital elevation model over South Africa based on ground and

satellite data', Boletim de Ciências Geo-désicas, vol. 28, Oct. 2022, https://doi.org/10.1590/s1982-2170202200030015.

12. M. Foumelis et al., 'Esa Snap - Stamps Integrated Processing for Sentinel-1 Persistent Scatterer Interferometry', in IGARSS 2018 - 2018 IEEE International Geoscience and Remote Sensing Symposium, Valencia: IEEE, Jul. 2018, pp. 1364–1367. https://doi.org/10.1109/IGARSS.2018.8519545.
13. A. Hooper, D. Bekaert, K. Spaans, and M. Arıkan, 'Recent advances in SAR interferometry time series analysis for measuring crustal deformation', Tectonophysics, vol. 514–517, pp. 1–13, Jan. 2012, https://doi.org/10.1016/j.tecto.2011.10.013.
14. Z. Yunjun, H. Fattahi, and F. Amelung, 'Small baseline InSAR time series analysis: Unwrapping error correction and noise reduction', Computers & Geosciences, vol. 133, p. 104331, Dec. 2019, https://doi.org/10.1016/j.cageo.2019.104331.
15. C. Werner, U. Wegmüller, T. Strozzi, and A. Wiesmann, 'Gamma SAR and Interferometric Processing Software', 2000.
16. U. Wegnüller, C. Werner, T. Strozzi, A. Wiesmann, O. Frey, and M. Santoro, 'Sentinel-1 Support in the GAMMA Software', Procedia Computer Science, vol. 100, pp. 1305–1312, 2016, https://doi.org/10.1016/j.procs.2016.09.246.
17. P. A. Rosen, E. Gurrola, G. F. Sacco, and H. Zebker, The InSAR scientific computing environment, paper presented at EUSAR 2012, 23-26 April 2012. 2012.